ARTICLE

Reducing the Adhesion between Surfaces Using Surface Structuring with PS Latex Particle

Jérôme Dejeu,[†] Mikhael Bechelany,*[,‡] Laetitia Philippe,[‡] Patrick Rougeot,[†] Johann Michler,[‡] and Michaël Gauthier*[,†]

FEMTO-ST Institute, UMR CNRS 6174-UFC/ENSMM/UTBM, 24 rue Alain Savary, 25000 Besançon, France, and EMPA-Materials Science & Technology, Mechanics of Micro - Materials and Nanostructures, Feuerwerkerstrasse 39, CH-3602 Thun, Switzerland

ABSTRACT The adhesion between a micro-object and a microgripper end-effector is an important problem in micromanipulation. Canceling or reducing this force is a great challenge. This force is directly linked to the surface chemical structure of the object and the gripper. We propose to reduce the adhesion force by using a self-assembled monolayer structuring on one surface. The surface was structured by polystyrene latex particles (PS particles) with radii from 100 to 1500 nm. The adhesion force measurements obtained by AFM were compared to a multisphere van der Waals force model. The model suggests the existence of an optimal value of the sphere radius which minimizes the adhesion. In that case, the pull-off force is reduced to 20 nN by the PS particles layer with a radius of 45 nm. A wide range of applications in the field of telecommunications, bioengineering, and more generally speaking, MEMS can be envisaged for these substrates.

KEYWORDS: surface structuring • adhesion force • pull-off force • PS latex particles • micromanipulation

INTODUCTION

The miniaturization of devices in the fields of telecommunication, bioengineering, and more generally speaking, of micro-electro-mechanical-systems (MEMS) is increasing and the assembly of these microproducts is a great challenge because of the microscopic size of the components (1). During robotic microassembly, microparts have to be picked, moved, and released. Other tasks like insertion, alignment, and guiding often must also be done. A contact between two surfaces, for example, gripping tools and a manipulated object or a substrate and a manipulated object, generates adhesion force and the influence of this force increases as the micro-object size decreases (2−4). The manipulation of a micro-object requires handling, positioning, and release without disturbances of the surface forces including electrostatic, van der Waals, or capillary forces.

Current microhandling methods are able to improve micromanipulation but the object behavior is always disturbed by adhesion and thus the repeatability and reliability is still low (5, 6). The required force to separate two surfaces is commonly called the "pull-off" force. The "pull-in" force is the attractive force between two objects when they approach closely. The pull-off forces are not well understood and must be studied further to enable the advent of reliable micromanipulation techniques. Current methods to measure micro/nanoforces between surfaces are the Surface Force Apparatus (SFA) (7, 8), the Atomic Force Microscope (AFM) (9−11), capacitive force sensors (12) or nanoindentation testers (13, 14).

The modeling of pull-off force are mainly based on two different approaches based on the surface energies on the contact (15−18) or on the integration of the van der Waals forces between objects (19−21) and on some hybrid approaches between both (23, 24).

We propose to control the surface forces between objects and grippers by surface nanostructure arrays in order to decrease the adhesion. The authors have already demonstrated that surface chemical functionalization can decrease adhesion forces (9) and switch them (25) in air and dry mediums, respectively. Thanks to the surface structures, we can reduce the contact area between the gripper and the object, and in turn this will decrease contact and van der Waals forces. Also, we can engineer specific properties of the gripper such as using electrically conductive materials to minimize electrostatic forces. In practice, the approach for surface structuring can be categorized into two directions: top-down and bottom-up approaches. Top-down approaches encompass lithographic and template-based techniques (26) and plasma treatment of the surfaces (27). Bottom-up approaches involve mostly self-assembly and self-organization (28) as for instance chemical deposition (29), layer-by-layer (LBL) deposition (30), hydrogen bonding (31), and colloidal assemblies (32). There are also methods based on the combination of both bottom-up and top-down approaches, for example, casting of polymer solution and phase separation (33), and electrospinning (34). Among

* Corresponding author. E-mail: mikhael.bechelany@empa.ch (M.B.); michael.gauthier@femto-st.fr (M.G.).
Received for review February 23, 2010 and accepted May 12, 2010
[†] FEMTO-ST Institute.
[‡] EMPA.
DOI: 10.1021/am100156c

Published on Web 06/02/2010

Table 1. Spin-Coating Parameters versus the PS Particle Radius

r_2 (nm)	step 1 (rpm for 10 s)	step 2 (rpm for 30 s)
100	200	1000
500	300	500
1500	300	400

these methods, the application using two-dimensional (2D) colloidal crystals, "natural lithography", which has been suggested by Deckman and Dunsmuir (35), has attracted attention because of it being a relatively easy process in comparison with conventional lithography (35). On the basis of such a process, uniformly sized microstructures could be produced on a substrate using a monolayer coating of colloidal spheres instead of a conventional resist. In recent years, various techniques, which are often called "colloidal lithography" or "nanosphere lithography", have been reported for nano/microfabrication or nano/micropatterning of a wide variety of solid substrates including semiconductors (36−40), metals (41), and ceramics.

The objective of this article is to measure and to model the adhesive force (pull-off) between a cantilever and a silicon surface strutured with regular arrays of polystyrene (PS) latex particles. The spheres are chosen because they allow us to develop a model to predict the evolution of the adhesion as a function of the scale effect. The adhesive force must be determined during the micromanipulation task. First, we present a surface patterning method then the adhesion measurement methodology. This is followed by a discussion of the force−distance measurements that were performed by AFM with a sphere glued on the cantilever extremity. Finally, the results are discussed in view of their applications in micromanipulation tasks. The array of spheres allows us to identify a particular size that achieves a minimal pull-off force.

MATERIALS AND METHODS

Surface Structuring. Three different types of commercially available PS microsphere suspension ($r_2 \approx 100$ nm, 2.53 wt % aqueous dispersion), ($r_2 \approx 500$ nm, 2.53 wt % aqueous dispersion) and ($r_2 \approx 1500$ nm, 2.53 wt % aqueous dispersion) were used (Polysciences, Inc., Eppelheim, Germany) as received. Acetone, NH_4OH (25%) and H_2O_2 (30%) were purchased from Aldrich and p-type Si wafers (5−10 Ω cm, (111) crystal orientation) of dimensions 1.5 cm^2 from Silicon Materials were used as substrates. Prior to patterning, the Si specimens were precleaned in acetone to remove the organic contaminants and then heated in air at 600 °C for 10 min to increase the thickness of the oxide layer. After that, the substrate was treated by the conventional RCA I process to obtain a hydrophilic Si surface, i.e., a treatment with a 1:1:5 solution of NH_4 OH (25%), H_2 O_2 (30%), and water at 80 °C for 15 min just before use was carried out (40). ***Note:*** *Piranha solution is highly corrosive and extremely reactive with organic substances; therefore, gloves, goggles, laboratory coats, and face shields are used while handling.* Hydrophilic surfaces were formed by the terminal silanol (SiOH) groups. After this pretreatment, a monodisperse suspension of polystyrene (PS) microspheres was spin-coated onto the substrate and after the suspension was dried in air at room temperature (RT). The spin coating was performed by controlling the parameters (time, speed and cycles) and are detailed in Table 1. After the complete evaporation of the solvent, the Si substrate with the binary colloidal crystals formed by the spheres was heated at 100 °C for 1 h, which is higher than the glass transition point ($T_g \approx 93$ °C) of polystyrene. This was done to increase the adhesive stability of the PS spheres on the Si surface.

After spin-coating, the PS spheres organized on the Si substrate were characterized by scanning electron microscopy (SEM, Hitachi S-4200, S-4800).

Force-Distance Measurement by Atomic Force Microscopy. Characterization of the pull-off force was performed with a commercial atomic force microscope (stand-alone SMENA scanning probe microscope NT-MDT). The experiments were done under a controlled environment with a laminar flow (humidity 30% and temperature 25 °C) on the Nanorol platform Station. The "Nanorol platform" can be used by external persons. The availability and the booking of the station is consultable via the Internet at http://nanorol.cnrs.fr/events.php.

The rectangular silicon AFM cantilever, whose stiffness is 0.3 N/m, was fixed and the substrate moved vertically. The same cantilever was used for all experiments. As the objective of this work is to improve the reliability of micro-object manipulation, interactions have been studied between a micrometric sphere and a plane. Measurements were in fact performed with a cantilever where a borosilicate sphere ($r_1 = 5$ μm radius) was glued in place of the standard AFM tip (ref*PT.BORO.SI.10*, company Novascan Technologies, Ames, IA,). Ten measurements were done at different locations on the same sample with a driving speed of 200 nm/s.

Typical Force−Distance Curve. The attractive and adhesive force−distance curve is presented in Figure 1. In this case, an attractive force (pull-in force) is measured when the sphere is coming close to the substrate (near −20 nN, Figure 1). In Figure 1, we are clearly measuring a pull-off force that represents the adhesion between the borosilicate sphere on the tip and the substrate. In this example, the pull-off force reaches −1.1 μN. This behavior represents an attraction between the surfaces.

RESULTS AND DISCUSSION

Microscopy. Monolayers of polystyrene PS spheres were created by spin coating PS spheres radius of 100, 500, and 1500 nm (Figure 2) onto a (111) Si/SiO_2 substrate. The heating of the structured surface was necessary in order to adhear the particle to the substrate. Indeed, without this step, it is impossible to scan the sample with particles because they moved along the surface.

The specimens were successfully coated with large domains of defect-free packing over the entire substrate surface. In Figure 2, the spheres arranged themselves into a close-packed structure of two-dimensional ordered lattices due to attractive capillary forces.

Force Measurement. Experiments have been done in a dry controlled medium with a structured surface by PS

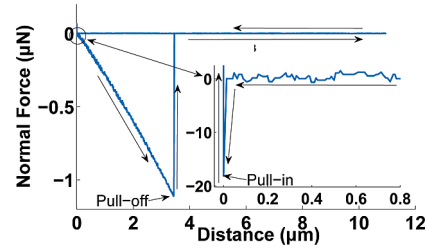

FIGURE 1. Attractive and adhesive typical force−distance curves between substrate and cantilever (stiffness 0.3 N/m).

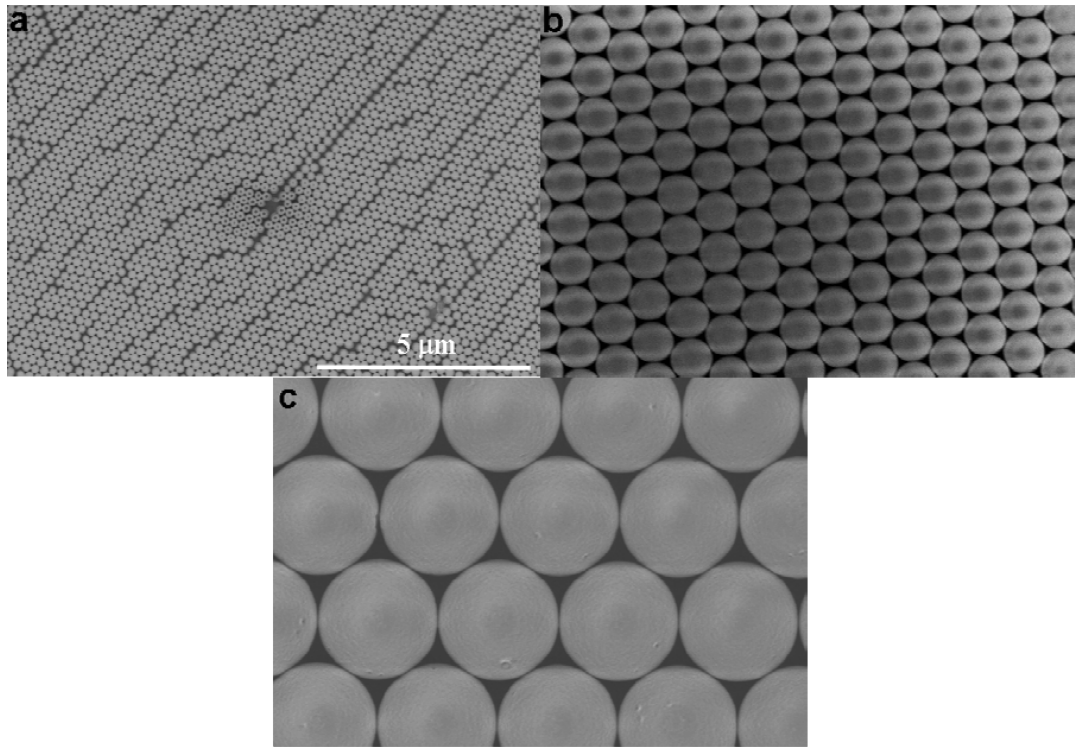

FIGURE 2. SEM images of a self-assembled monolayer of PS spheres with a radius of (a) 100, (b) 500, and (c) 1500 nm.

latex particles and a borosilicate sphere on the cantilever tipless AFM cantilever. The measurements were repeated ten times on the same points and at different point of the sample. Additionally, measurements on the different particles sizes have been done. Examples of the force distance measurements in each sample are presented in Figure 3 and discussed below.

The average values of the different measurements presented in Figure 3, (pull-in and pull-off forces), for different PS latex particles size, are summarized in Table 2.

The PS particle deposition decreases the pull-off force compared to the uncoated silica surface (−386 nN as opposed to −1 μN). The size of the PS latex particles has an important influence on the adhesion. Indeed, decreasing the size from 1500 μm to 100 nm reduces the adhesion force nearly 10 times. However, the pull-in force, e.g., the force when two surfaces approach one another, was roughly −6 nm for all the PS particles. This phenomenon can be explain by the fact that the experiment was performed in air, so there are no important charges on the surface, except charges induced by humidity.

Results Analysis. ***Number of Contact Points.*** Usually force measurements are conducted between a sphere and an planar substrate where the contact surface is necessary a unique surface. In our case, the substrate is structured with several microspheres and the numbers of contacts must be studied.

The relative position between the probe and the spheres on the substrate is described in Figure 4. When the probe is approaching, it touches a first sphere S_a. The distance between the probe and the second sphere S_b is called z_b. During force measurement, a preload force is applied on the sphere which induces a local deformation defined by the displacement δ. If δ is less than the distance z_b, the probe does not touch the second sphere S_b and the contact is a sphere−sphere contact.

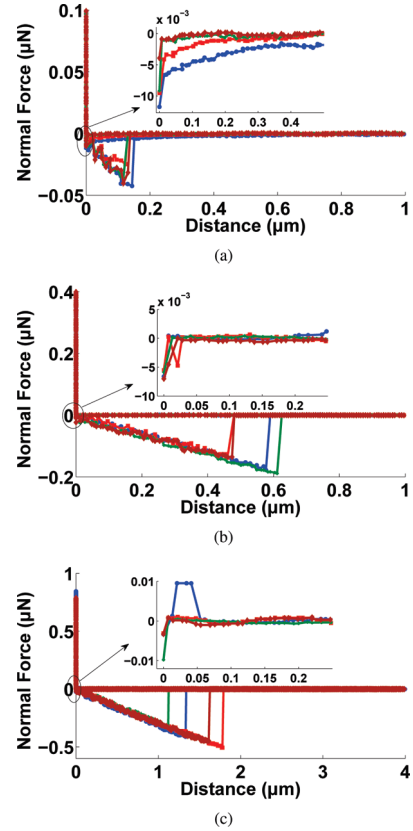

FIGURE 3. Force−distance curves, in dry medium, for a structured surface by differents PS latex particles size (stiffness: 0.3 N/m) with a radius of (a) 100, (b) 500, and (c) 1500 nm.

Table 2. Influence of the PS Particles Size on the Pull-in and Pull-off Forces (nN) (stiffness 0.3 N/m)

r_2 (nm)	pull-in (nN)	pull-off (nN)
particle-free silica	0	>−1000
100	−8.7 ± 1.5	−33.5 ± 7
500	−6.0 ± 1.7	−159 ± 24
1500	−5.9 ± 3.6	−386 ± 67

We are going to show that in a large majority of cases, the displacement δ is negligible compared to the distance z_b. The distance d between the probe and the second sphere is a function of the relative position of the probe and the PS spheres. The maximum value z_{bmax} of z_b is reached when the probe and the first sphere are aligned:

$$z_b \in (0; z_{bmax} = r_2 - \sqrt{r_2^2 - 2r_1^2}) \tag{1}$$

As the Tabor parameter (18), is from 8.6 to 19, the JKR model (15) should be considered in order to estimate the displacement δ. In the case of a sphere−sphere contact, the displacement δ is given by:

$$\delta = \frac{a^2}{r_{12}} - \sqrt{\frac{4F_{\text{pull-off}}a}{3E^* r_{12}}} \tag{2}$$

$$a^3 = \frac{3r_{12}}{4E^*}(F_{\text{ext}} + 2F_{\text{pull-off}} + 2\sqrt{F_{\text{pull-off}}F_{\text{ext}} + (F_{\text{pull-off}})^2}) \tag{3}$$

where $F_{\text{pull-off}}$ is the pull-off force and F_{ext} is the external or load force applied on the sphere (22), the r_{12} is the relative radius and E^* is the effective Young's modulus defined by respectively:

$$\frac{1}{r_{12}} = \frac{1}{r_1} + \frac{1}{r_2} \tag{4}$$

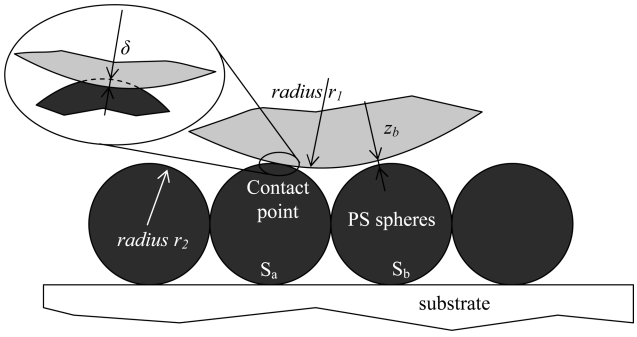

FIGURE 4. Description of the contact between the probe and the PS spheres on the substrate.

$$\frac{1}{E^*} = \frac{1 - \nu_1^2}{E_1} + \frac{1 - \nu_2^2}{E_2} \tag{5}$$

where E_i and ν_i are the Young's modulus and the Poisson's coefficient of the material i. Their values were, respectively, 3.2 GPa and 0.33 for the polystyrene sphere and 71 GPa and 0.21 for the borosilicate sphere. So, the effective Young's modulus is $E^* = 4.5$ GPa.

The Table 3 describes the deformation values δ induced only by adhesion corresponds to the value of δ when the external preload F_{ext} is null.

Table 3 shows that this deformation δ induced by adhesion is negligible compared to the maximal distance z_{bmax}. We consequently assume that the force measurements have been done on a unique contact point. Moreover as the distance between the second sphere z_{bmax} is greater than the typical interaction distance $z_0 \in$ [0.2 nm; 0.4 nm] at the contact, only the interaction between the probe and the first sphere can be considered.

Interaction Force Modeling. As the pull-off force is a direct consequence of van der Waals force between both objects, the experimental pull-off measurements can be compared with van der Waals models (19−21, 23, 24). This model has been chosen in spite of DMT or JKR model in order to build one which can be easily extended to smaller spheres. Indeed, we are going to show that in case of nanospheres (radius <100 nm), the distance interaction with more that one sphere in the plane should be considered. These distance forces can easily be taken into account using the van der Waals model. On the basis of ref 21, the impact of local deformation on the calculation of van der Waals force can be neglected in the nanoscale, thus we are considering the force between two rigid spheres:

$$F_{\text{vdw}} = \frac{A_{12}r_{12}}{6z_0^2} \tag{6}$$

where z_0 is the contact distance and A_{12} the Hamaker constant which can be calculated using the approximative combination law:

$$A_{12} = \sqrt{A_1 A_2} \tag{7}$$

where A_i is the Hamaker constant of the material i.

In our case, Hamaker constants of the polystyrene and of the silica are respectively $A_1 = 79$ zJ (42) and $A_2 = 65$ zJ (21). With these Hamaker values, the Hamaker constant

Table 3. Characterization of the Contact Deformation in Function of the PS Sphere Radius

r_2 (nm)	z_{bmax} (nm)	δ (nm)
100	4	1.4
500	100	2.5
1500	1×10^3	3.4

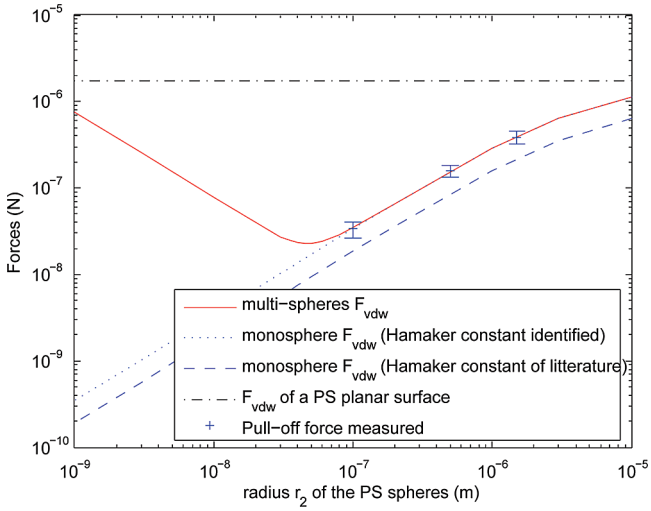

FIGURE 5. Experimental and theoretical forces as a function of the radius r_2 of the PS spheres: the dashed and dotted blue lines represent the monosphere model of the van der Waals force based respectively on the theoretical value (eq 7) and the identified value (eq 8), red solid line described the multisphere model which is similar to the monosphere model for r_2 greater than 100 μm. Error bars show the experimental measurements. The decreasing of the experimental pull-off force can be predicted by the models. Moreover, the multisphere model (red line) shows that the pull-off force reaches a minimum for $r_2 = 45$ nm. Below this value, the force is increasing and is converging to a PS plane interaction (dashdot line).

of the system determined with the approximate combination law (eq 7) is $A_{12} = 72$ zJ. The typical values of z_0 are between 0.2 nm and 0.4 nm, we assume that $z_0 = 0.25$ nm.

The Figure 5 presents the experimental forces as a function of the radius r_2. The van der Waals force (6) based on the combination law (7) and drawn in dashed line has the same tendency as the experimental values and the maximum error is around 30%. These values are also providing an opportunity to identify the Hamaker constant between polystyrene and borosilicate. RMSE optimization has enabled the determination of the Hamaker constant

$$A_{12}^{\mathrm{id}} = 1.29 \times 10^{-19}\,\mathrm{J} \tag{8}$$

Differences between the experimental and theoretical values of the Hamaker constant could be explained by the approximation made in the combination law (eq 7) and some uncertainties on the chemical composition of the silica. The van der Waals force calculated with this value is plotted as a dotted line in Figure 5. It shows that the model proposed in eq 6 is able to predict the pull-off force between the spherical probe and the structured surface.

Analysis of the Scale Effect. On the basis of the model (eq 6), the evolution of the interaction force can be extended to smaller spheres. In this case, the interaction force between the probe and the other spheres have to be considered. Let us consider the arrangement described in Figure 6, and the fact that the measurement is taken at the sphere defined by $(i = 0, j = 0)$. On the basis of a geometrical

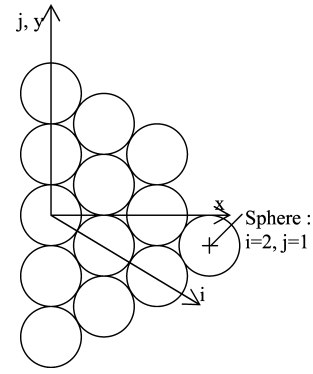

FIGURE 6. Arrangement of the PS spheres on the substrate.

analysis, the distance z_{ij} between the probe (r_1) and a sphere (i, j) is:

$$z_{ij} = \sqrt{(r_2 + z_0 + r_1)^2 + 4r_2^2(j^2 - ij + i^2)} - r_1 - r_2 \tag{9}$$

The van der Waals force z_{ij} between the probe and the sphere (i, j) verifies:

$$\|\vec{F}_{ij}\| = \frac{Ar_{12}}{6z_{ij}^2} \tag{10}$$

The total force F_{Tvdw} between an infinite plan structured with PS spheres and the probe is thus:

$$F_{\mathrm{Tvdw}} = \sum_{i,j}^{\mathbb{Z}^2} \vec{F}_{ij}\vec{z} \tag{11}$$

$$F_{\mathrm{Tvdw}} = \sum_{i,j}^{\mathbb{Z}^2} \frac{Ar_{12}}{6z_{ij}^2}\frac{r_2 + z_0 + r_1}{r_2 + z_{ij} + r_1} \tag{12}$$

This model of the interaction between a spherical probe and a structured surface has been simulated using the Matlab Simulink software. The evolution of F_{Tvdw} as a function of the radius, r_2, of the sphere is drawn as a red dashed line in Figure 5. It shows that the monosphere model proposed in eq 6 is valid for r_2 larger than 100 nm. For radii below 100 nm, the force induced by the spheres around the contact sphere cannot be neglected. The second results deals with the determination of a minimum of the interaction force which represents an optimum of adhesion reduction in the applicative field of micromanipulation. In our experimental case, the optimum radius r_2 in order to minimize the adhesion is 45 nm. This value depends of the diameter of borosilicate sphere glue to the cantilever. We can extend the model to different diameters of borosilicate sphere. If the radius is lower than this optimum, more and more spheres should be considered in the sum (eq 12), thus increasing the force. As the sphere radius approach 1 nm, the total force approaches the theoretical interaction force with an uniform

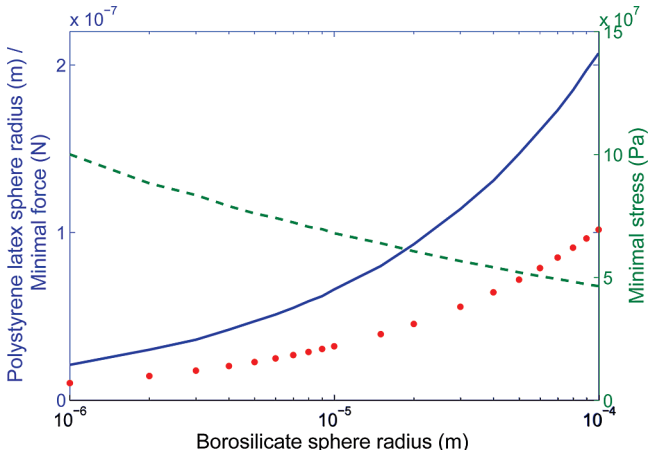

FIGURE 7. Simulation of the borosilicate radius influence on polystyrene latex sphere radius in order to obtain the minimal adhesion force. Minimal adhesion force variation (red dotted line), polystyrene latex radius obtained (blue solid line), and stress (green dashed lines) versus the borosilicate sphere.

planar surface of PS. It is possible to show that the interaction force between the substrate above the PS sphere and the borosilicate sphere is negligible for PS spheres whose radius r_2 is larger that 1 nm. For example, for small PS spheres whose radius is $r_2 = 5$ nm, the force F_{Tvdw} is $1.55e - 7$N and the interaction force between the borosilicate sphere $r_1 = 5\,\mu$m and the substrate above the PS spheres is $4.2e - 9$N.

We note here that researchers have developed arrays of polymer pillars (43) and vertically aligned carbon nanotubes (44) that stick firmly to surfaces (45). These surfaces structuring could validate our model that by decreasing the diameter of the PS spheres, we increase the adhesion forces. However, more experiments are in progress in order to synthesize PS spheres monolayer with diameters less than 100 nm and to study the adhesion forces on these monolayers.

The optimum radius r_2 and the minimal adhesion force obtained depends also on the radius r_1 of the borosilicate sphere. Figure 7 presents the simulation of the minimal pull-off force and the polystyrene radius r_2 associated versus the borosilicate radius r_1. In an applicative point of view, in micromanipulation, the pull-off force between the gripper and the object must be minimal. For each radius r_1 of manipulated borosilicate microspheres, Figure 5 gives the optimal radius r_2 of the PS structuration of the gripper and the pull-off force obtained. The contact pressure $F_{Tvdw}/\pi a^2$ is also described in Figure 7. Consequently, Figure 7 represents a relevant tool for the design of the surface structuration of microgrippers.

CONCLUSION

In this communication, we have studied the interaction behavior, i.e. the adhesion force, between a structured surface and a borosilicate sphere. The experiments were performed as a function of the polystyrene latex particle radii from 100 to 1500 nm deposited on the silica substrate. The PS sphere size influences the pull-off force, and the experimental decreasing of PS size decreases the adhesion force near 100 times compared to a uncoated substrate. A van der Waals model computing a mono- or multisphere approach and measurements were compared and show a good agreement with a maximal error less than 30 %. On the basis of the model, we have shown that the adhesion force could be minimized with a PS latex particle radius near to 45 nm.

More experiments are in progress in order to confirm this model. Because adhesion is the current highest disturbance in micromanipulation (positioning and releasing), structured surface is a promising way to improve micro-object manipulation in the future. This paper provides design rules to structure gripper surface in order to minimize adhesion. A wide range of applications, in the field of telecommunications, bioengineering, and more generally speaking, MEMS, can be also envisaged for these substrates.

Acknowledgment. This work was supported by the EU under HYDROMEL (Contract NMP2-CT-2006-026622), Hybrid ultra precision manufacturing process based on positional- and self-assembly for complex microproducts; and by the French National Agency (ANR) under NANOROL (Contract ANR-07-ROBO-0003), Nanoanalyse for micromanipulate. We also like acknowledge the support of Dr. Zhao WANG, EMPA, for his interaction model correction.

REFERENCES AND NOTES

(1) Tamadazte, B.; Dembélé, S.; Le Fort-Piat, N. *Sens. Transducers J.* **2009**, *5*, 37–52.
(2) Lambert, P. *Capillary Forces in Micro-assembly*; Springer: Amsterdam, The Netherlands, 2008.
(3) Gauthier, M.; Régnier, S.; Rougeot, P.; Chaillet, N. *J. Micromech.* **2006**, *3*, 389–413.
(4) Zhou, Q.; Chang, B.; Koivo, H. N. Ambient environment effects in micro/nano handling. *Proceedings of the International Workshop on Microfactories*; Shangai, China, Oct 15−17, 2004; IOP Publishing Ltd.: Bristol, U.K., 2004; pp 146−151.
(5) Hériban, D.; Gauthier, M. Robotic Micro-assembly of Microparts Using a Piezogripper. *Proceedings of the 2008 IEEE/RSJ International Conference on Intelligent Robots and Systems*; Nice, France, Sept 22−26, 2008; IEEE: Piscataway, NJ, 2008; pp 4042−4047.
(6) Dafflon, M.; Lorent, B.; Clavel, R. A micromanipulation setup for comparative tests of microgrippers. *International Symposium on Robotics (ISR)*; Rio de Janeiro, Brazil, July 6−10, 2006; International Federation of Robotics: Frankfurt, Germany, 2006; CD-ROM available on-line on EPEL website.
(7) Blomberg, E.; Poptoshev, E.; Claesson, P. M.; Caruso, F. *Langmuir* **2004**, *20*, 5432–5438.
(8) Charrault, E.; Gauthier, C.; Marie, P.; Schirrer, R. *Langmuir* **2009**, *25*, 5847–5854.
(9) Dejeu, J.; Rougeot, P.; Gauthier, M.; Boireau, W. *Micro Nano Lett* **2009**, *4*, 74–79.
(10) Wang, T.; Canetta, E.; Weerakkody, T. G.; Keddie, J. L. *ACS Appl. Mater. Interfaces* **2009**, *1*, 631–639.
(11) Gong, H.; Garcia-Turiel, J.; Vasilev, K.; Vinogradova, O. I. *Langmuir* **2005**, *21*, 7545–7550.
(12) Rabenorosoa, K.; Clevy, C.; Lutz, P.; Gauthier, M.; Rougeot, P. *Micro Nano Lett.* **2009**, *4*, 148–154.
(13) Vajpayee, S.; Hui, C.-Y.; Jagota, A. *Langmuir* **2008**, *24*, 9401–9409.
(14) Murphy, M. P.; Kim, S.; Sitti, M. *ACS Appl. Mater. Interfaces* **2009**, *1*, 849–855.
(15) Johnson, K. L.; Kendall, K.; Roberts, A. D. *Proc. R. Soc. London, Ser. A* **1971**, *324*, 301–313.
(16) Derjaguin, B. V.; Muller, V.; Toporov, Y. P. *J. Colloid Interface Sci.* **1975**, *53*, 314–326.
(17) Maugis, D. *J. Colloid Interface Sci.* **1992**, *150*, 243–269.

(18) Maugis., D. *Contact, Adhesion and Rupture of Elastic Solids*; Springer Series in Solid-State Sciences; Springer: New York, 2000.
(19) Hamaker, H. C. *Physica* **1937**, *4*, 1058.
(20) Delrio, F. W.; Boer, M. P. D.; Knapp, J. A.; David Reedy, E.; Clews, P. J.; Dunn, M. L. *Nat. Mater.* **2005**, *4*, 629–634.
(21) Alvo, S.; Lambert, P.; Gauthier, M.; Régnier, S. *J. Adhes. Sci. Technol.* **2010**, in press.
(22) Israelachvili, J. *Intermolecular and Surface Forces*, second ed.; Academic Press: New York, 1991.
(23) Thoreson, E.; Martin, J.; Burnham, N. *J. Colloid Interface Sci.* **2006**, *298*, 94–101.
(24) Li, Q.; Rudolph, V.; Peukert, W. *Powder Technol.* **2006**, *161*, 248–255.
(25) Dejeu, J.; Rougeot, P.; Gauthier, M.; Boireau, W. *ACS Appl. Mater. Interfaces* **2009**, *1*, 1966–1973.
(26) Li, J.; Fu, J.; Cong, Y.; Wu, Y.; Xue, L. J.; Han, Y. C. *Appl. Surf. Sci.* **2006**, *252*, 2229–2234.
(27) Kim, S. H.; Kim, J. H.; Kang, B. K.; Uhm, H. S. *Langmuir* **2005**, *21*, 12213–12217.
(28) Han, J. T.; Zheng, Y.; Cho, J. H.; Xu, X.; Cho, K. *J. Phys. Chem. B* **2005**, *109*, 20773–20778.
(29) Zhao, N.; Shi, F.; Wang, Z. Q.; Zhang, X. *Langmuir* **2005**, *21*, 4713–4716.
(30) Shi, F.; Wang, Z. Q.; Zhang, X. *Adv. Mater.* **2005**, *17*, 1005–1009.
(31) Han, J. T.; Lee, D. H.; Ryu, C. Y.; Cho, K. W. *J. Am. Chem. Soc.* **2004**, *126*, 4796–4797.
(32) Hikita, M.; Tanaka, K.; Nakamura, T.; Kajiyama, T.; Takahara, A. *Langmuir* **2005**, *21*, 7299–7302.
(33) Jiang, L.; Zhao, Y.; Zhai, J. *Angew. Chem., Int. Ed.* **2004**, *43*, 4338–4341.
(34) Gu, Z. Z.; Wei, H. M.; Zhang, R. Q.; Han, G. Z.; Pan, C.; Zhang, H.; Tian, X. J.; Chen, Z. M. *Appl. Phys. Lett.* **2005**, *86*, 201915.
(35) Deckman, H.; Dunsmuir, J. *Appl. Phys. Lett.* **1982**, *41*, 377.
(36) Sakamoto, S.; Philippe, L.; Bechelany, M.; Michler, J.; Asoh, H.; Ono, S. *Nanotechnology* **2008**, *19*, 405304–405309.
(37) Bechelany, M.; Brodard, P.; Philippe, L.; Michler, J. *Nanotechnology* **2009**, *20*, 455302–455309.
(38) Bechelany, M.; Maeder, X.; Riesterer, J.; Hankache, J.; Lerose, D.; Christiansen, S.; Michler, J.; Philippe, L. *Cryst. Growth Des.* **2010**, 587–596.
(39) Elias, J.; Lévy-Clément, C.; Bechelany, M.; Michler, J.; Wang, G.-Y.; Wang, Z.; Philippe, L. *Adv. Mater.* **2010**, *22*, 1607–1612.
(40) Mook, W.; Niederberger, C.; Bechelany, M.; Philippe, L.; Michler, J. *Nanotechnology* **2010**, *21*, 55701.
(41) Huang, Z.; Fang, H.; Zhu, J. *Adv. Mater.* **2007**, *19*, 744–748.
(42) Parsegian, A. *Van der Waals forces: a Handbook for Biologists, Chemists, Engineers, And Physicists*; Cambridge University Press: New York, 2005.
(43) Geim, A. K.; Dubonos, S. V.; Grigorieva, I. V.; Novoselov, K. S.; Zhukov, A. A.; Shapoval, S. Yu *Nat. Mater.* **2003**, *2*, 461–463.
(44) Qu, L.; Dai, L. M. *Adv. Mater.* **2007**, *19*, 3844–3849.
(45) Wang, Z. L. *Nat. Nanotechnol.* **2009**, *4*, 407–408.

AM100156C